Structure of macrophage colony stimulating factor bound to FMS: Diverse signaling assemblies of class III receptor tyrosine kinases

Xiaoyan Chen, Heli Liu, Pamela J. Focia, Ann Hye-Ryong Shim, and Xiaolin He[1]

Department of Molecular Pharmacology and Biological Chemistry, Feinberg School of Medicine, Searle 8-417, Northwestern University, 303 East Chicago Avenue, Chicago, IL 60611

Edited by Pamela J. Bjorkman, California Institute of Technology, Pasadena, CA, and approved October 14, 2008 (received for review August 7, 2008)

Macrophage colony stimulating factor (M-CSF), through binding to its receptor FMS, a class III receptor tyrosine kinase (RTK), regulates the development and function of mononuclear phagocytes, and plays important roles in innate immunity, cancer and inflammation. We report a 2.4 Å crystal structure of M-CSF bound to the first 3 domains (D1–D3) of FMS. The ligand binding mode of FMS is surprisingly different from KIT, another class III RTK, in which the major ligand-binding domain of FMS, D2, uses the CD and EF loops, but not the β-sheet on the opposite side of the Ig domain as in KIT, to bind ligand. Calorimetric data indicate that M-CSF cannot dimerize FMS without receptor-receptor interactions mediated by FMS domains D4 and D5. Consistently, the structure contains only 1 FMS-D1–D3 molecule bound to a M-CSF dimer, due to a weak, hydrophilic M-CSF:FMS interface, and probably a conformational change of the M-CSF dimer in which binding to the second site is rendered unfavorable by FMS binding at the first site. The partial, intermediate complex suggests that FMS may be activated in two steps, with the initial engagement step distinct from the subsequent dimerization/activation step. Hence, the formation of signaling class III RTK complexes can be diverse, engaging various modes of ligand recognition and various mechanistic steps for dimerizing and activating receptors.

growth factor | signal transduction

Macrophage colony-stimulating factor (M-CSF), also known as colony-stimulating factor-1 (CSF-1, as encoded by the *Csf1* gene), is the primary cytokine that regulates the survival, proliferation, differentiation and function of the cells of the mononuclear phagocyte lineage (1). The effects of M-CSF are mediated by its cell-surface receptor FMS (also known as the CSF-1 receptor, or CSF-1R), a receptor tyrosine kinase (RTK) encoded by the *c-fms* proto-oncogene, the human homologue of the *v-fms* oncogene from the Susan McDonough strain of feline sarcoma virus (2, 3). In immune response and inflammation, M-CSF/FMS signaling activates monocytes and macrophages by enhancing their cytotoxicity, phagocytosis, chemotaxis, and cytokine production and modulates the development and function of dendritic cells (4). The M-CSF/FMS autocrine loop is also a key regulator of brain inflammation response as mediated by microglia, the resident macrophage in the central nervous system (4). In addition to their crucial roles in inflammation and innate immunity, M-CSF and FMS are also important in bone metabolism (5), female reproduction (6), and lipoprotein clearance (7). Abnormal M-CSF/FMS signaling is implicated in a wide range of inflammatory disorders such as arthritis (8), atherosclerosis (9), and obesity (10). It is also involved in tumor growth (11) and metastasis (12, 13).

M-CSF functions as a homodimer, and exists in at least three forms, secreted glycoprotein, secreted proteoglycan, and cell-surface glycoprotein, as a result of alternative mRNA splicing (14) and posttranslational modification (15). All forms contain the N-terminal receptor-binding domain and the C-terminal transmembrane domain with variable inserts between these two parts. Soluble forms of M-CSF are released by proteolysis. M-CSF belongs to a small group of short-chain 4-helix bundle, RTK-binding cytokines, which also includes stem cell factor (SCF) and FLT3L (16). The core receptor-binding domains of these three cytokines have a similar head-to-head dimeric structure (17–20). In addition, they bind the same group of cell surface receptors, the class III RTKs (21).

The class III RTKs, including FMS, KIT (the receptor for SCF), FLT3 (the receptor for FLT3L), and PDGFR-α and -β, are composed of a glycosylated extracellular segment with 5 Immunoglubulin (Ig)-like domains, a single transmembrane segment, and a split intracellular kinase domain (21). Binding of ligands to the class III RTKs leads to receptor dimerization, intermolecular autophosphorylation and kinase domain activation. The structure of the receptor/ligand complex for one of the class III RTKs, KIT, has been determined (22, 23), demonstrating that the dimerization of KIT is exclusively driven by bivalent binding of SCF to its first 3 Ig domains, and the correct positioning of membrane-proximal domains is critical for activation. Because KIT is homologous to other class III RTKs, it is believed that ligand recognition and signaling assembly of KIT, and the mechanism of dimerization and activation of KIT are representative of the entire family of class III RTKs (22, 23). In particular, FMS is the closest KIT relative, and previous biochemical data indicated its ligand-binding properties and domain contributions are similar to KIT (24, 25). However, a structural proof of such a similarity is lacking.

In this article, we have determined the crystal structure of the complex between M-CSF and the first three domains of FMS, showing that the ligand-binding mode, surprisingly, is not conserved among class III RTKs. This structure, in combination with thermodynamic evidence, provides insight into the dimerization and activation mechanisms of this important class of receptors.

Results and Discussion

Reconstitution of the M-CSF:FMS Complexes. We expressed the receptor-binding domain of mouse M-CSF, and the N-terminal three domains (D1–D3) and the entire extracellular segment (D1-D5) of mouse FMS, using insect cells. The complexes were formed by mixing the ligand and the receptor at a 1:1 molar ratio, and analyzed by size exclusion chromatography. We found a

Author contributions: X.C. and X.H. designed research; X.C., H.L., and A.H.-R.S. performed research; X.C., P.J.F., and X.H. analyzed data; and X.C. and X.H. wrote the paper.

The authors declare no conflict of interest.

This article is a PNAS Direct Submission.

Data deposition: The coordinates and structure factors have been deposited in the Protein Data Bank, www.pdb.org (PDB ID code 3EJJ).

[1]To whom correspondence should be addressed. E-mail: x-he@northwestern.edu.

This article contains supporting information online at www.pnas.org/cgi/content/full/0807762105/DCSupplemental.

BIOCHEMISTRY

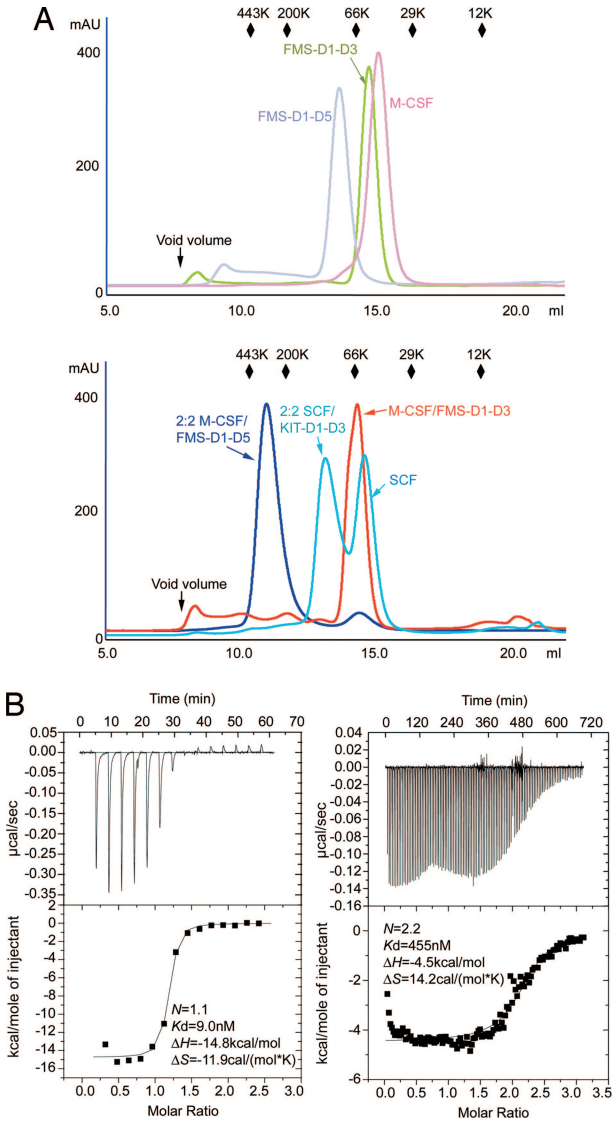

Fig. 1. Stoichiometry and binding between M-CSF and FMS. (*A*) Gel filtration analysis of M-CSF, FMS, and the M-CSF:FMS complexes in a calibrated Superdex-200 column equilibrated and eluted with HBS buffer [10 mM Hepes (pH 7.5), 150 mM NaCl]. (*Upper*) Pink, M-CSF; green, FMS-D1–D3; lavender, FMS-D1-D5. (*Lower*) Red, M-CSF:FMS-D1–D3; blue, M-CSF:FMS-D1-D5; cyan, the 2:2 SCF:KIT complex and free SCF for comparison. (*B*) Thermodynamical profiles of M-CSF:FMS binding measured by calorimetry. M-CSF was injected into FMS-D1-D5 (*Left*) and FMS-D1–D3 (*Right*) in 2 separate experiments. The stoichiometry (*N*), affinity (K_d), enthalpy change (ΔH) and entropy change (ΔS) of each binding experiment are listed by the fitted curves.

major difference between the elution volumes of the M-CSF:FMS-D1–D3 complex and the M-CSF:FMS-D1-D5 complex (Fig. 1*A*). The apparent size of M-CSF:FMS-D1-D5 was 200–300 kDa, larger than the size calculated for a 2:2 complex (≈150 kDa), nevertheless consistent with the likely extended shape of the complex. The size of the M-CSF:FMS-D1–D3 complex appeared to be <66 kDa, whereas an assumed 2:2 complex would have an expected size of ≈100 kDa. In comparison, the 2:2 complex between SCF and KIT-D1–D3 eluted much earlier (Fig. 1*A*). The small apparent size of the M-CSF:FMS-D1–D3 complex suggests the possibility that the gel filtration peak either is a mixture of dissociated M-CSF dimers and FMS monomers, or represents a complex containing <2 M-CSF plus 2 FMS-D1–D3 molecules.

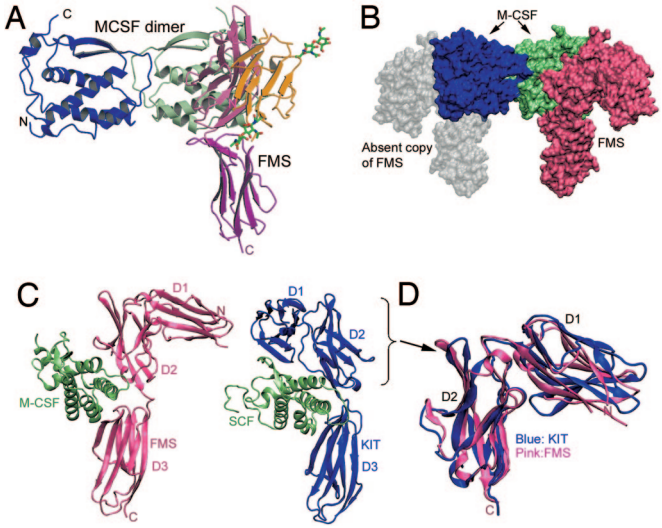

Fig. 2. Structure of the M-CSF:FMS-D1–D3 complex. (*A*) Ribbons representation of the complex, with the 2 M-CSF protomers in green and blue, and the FMS D1, D2, and D3 domains in orange, pink, and purple, respectively. The 2 N-linked glycans attached to FMS are depicted as sticks. (*B*) Surface representation of a completed, 2:2 M-CSF:FMS-D1–D3 complex in which the absent copy of FMS-D1–D3 (gray) is modeled based on the 2-fold symmetry between the 2 M-CSF protomers. (*C*) The different modes of ligand recognition between FMS and KIT as revealed by a comparison between M-CSF:FMS-D1–D3 (*Left*) and SCF:KIT-D1–D3 (*Right*) complexes. For clarity only one pair of receptor and ligand from each complex is shown. The ligands are in the same orientation. (*D*) Superimposition of FMS-D1-D2 and KIT-D1-D2 showing that D1 and D2 form an integral, rigid module.

To characterize the M-CSF:FMS-D1–D3 and M-CSF:FMS-D1-D5 complexes, we measured the binding between M-CSF and FMS-D1–D3 versus the binding between M-CSF and FMS-D1-D5 using isothermal titration calorimetry (ITC). Titrating the M-CSF protein into the FMS proteins revealed that FMS-D1-D5 was saturated by equal molar amounts of M-CSF, but FMS-D1–D3 was saturated by double amounts of M-CSF (Fig. 1*B Left* and *Right*). This, together with the apparent sizes determined by size exclusion chromatography, suggests it is likely that the stoichiometry of the M-CSF:FMS-D1-D5 complex is 2:2, but that of the M-CSF:FMS-D1–D3 complex is 2:1. This suggests that in the absence of domains D4 and D5, FMS can only form a partial complex with M-CSF, leaving one of the FMS-binding sites on the M-CSF dimer unoccupied. The D4 and D5 domains could, thus, mediate additional interactions that enable dimerization. Indeed, M-CSF binds to FMS-D1-D5 with ≈50-fold higher affinity than to FMS-D1–D3. The M-CSF:FMS-D1-D5 binding is significantly more enthalpically favored (−14.8 vs. −4.5 kcal/mol) than the M-CSF:FMS-D1–D3 binding, albeit slightly entropically disfavored as opposed to being slightly favored in the M-CSF:FMS-D1–D3 binding. This strong enthalpic enhancement suggests that the FMS D4 and D5 domains contribute extensive hydrophilic interactions during the formation of the full-length signaling complex.

Structure of the M-CSF:FMS-D1–D3 Complex. The M-CSF:FMS-D1–D3 complex was crystallized with a mixture of purified M-CSF and FMS at a 1:1.2, but not 2:1, molar ratio. The excess FMS-D1–D3 was intended to force the formation of a full, 2:2 complex. However, the structure determination unambiguously revealed 2 molecules of M-CSF and only 1 molecule of FMS-D1–D3 in the asymmetric unit (Fig. 2*A*). The potential binding of FMS-D1–D3 at the second FMS-binding site on the M-CSF

dimer (Fig. 2*B*), undetectable by calorimetry, is probably weaker than crystal packing.

The 2:1 M-CSF:FMS-D1–D3 complex contains a head-to-head M-CSF dimer and a monomeric FMS bound to the side of 1 M-CSF protomer, with the symmetry-related, equivalent FMS-binding site of the second M-CSF protomer unoccupied. M-CSF binds exclusively to the D2 and D3 domains of FMS, unlike the SCF:KIT binding, which additionally involves D1 of KIT (22, 23) (Fig. 2*C*). The approximately straight D2 and D3 domains run perpendicular to the long dimension of M-CSF dimer, contacting M-CSF with the regions around the D2-D3 junction. The D1 domain is angled ≈100° from D2 in the direction opposite to M-CSF. Two additional domains, D4 and D5, not present in the structure, presumably extend from the D3 C terminus to the cell-surface. The M-CSF structure, as in the free human M-CSF structure (18), has a core of 4 α-helices (A–D) and 2 β-strands (β1 and β2). The backbone of the M-CSF protomer is similar to the backbone of free human M-CSF (18), with only minor deviations located at the segment linking helix C and the β2 strand around the tail of the M-CSF dimer (superimposition of Cα atoms yielded a rmsd of 0.8 Å); the head-to-head dimerization mode of M-CSF is also unchanged in the complex.

The structure of FMS-D1–D3 is bent ≈100° between domains D1 and D2, but is approximately straight between domains D2 and D3 (Fig. 2*C*). D1 is a small I-set Ig domain, with a typical 3-on-four (ABED on GFC) β-sheet bilayer configuration and part of the A strand (A′) moved to the GFC layer. The FG loop (residues 88–94) of D1 is disordered. D2 is a distorted I-set Ig domain, with its GFC layer twisted into two separate β-sheets: the lower sheet forms a bilayer with the BED β-sheet; the upper sheet, together with the GFC β-sheet of D1, serves to sandwich the irregular region around the D1-D2 junction into a rigid structure. The D1 and D2 domains hence form an integral structural component, reinforced by numerous, mostly hydrophobic D1-D2 interactions (Fig. 2*D*). A total of 1,240 Å^2 surface area is buried at the D1-D2 junction. The D3 domain is a canonical I-set Ig domain. The D2-D3 junction is minimal, with few interactions between D2 and D3. Without the binding of M-CSF, the D2-D3 junction likely has hinge flexibility.

The partial, 2:1 M-CSF:FMS complex likely represents a stable intermediate state during receptor dimerization. A full, 2:2 complex can be modeled by applying the 2-fold symmetry between two M-CSF protomers to FMS. When the absent copy of FMS is added to the unoccupied site on the M-CSF dimer, the structure resembles the letter H with its top pushed down (Fig. 2*B*), similar to the symmetrical SCF:KIT complex. The overall shape of the 2:2 M-CSF:FMS complex appears much wider than the 2:2 SCF:KIT complex, due to the swung-out D1 domains. Although the second FMS-binding site on the M-CSF dimer is not used in this complex, it may not be completely disabled, but perhaps rendered into a low-affinity state. For FMS to become activated, additional factors are likely needed to cause FMS to dimerize.

The M-CSF:FMS binding mode is dramatically different from the SCF:KIT binding mode (Fig. 2*C*). KIT binds SCF in a "wrapping" fashion, with all 3 of the first domains (D1–D3) interacting with SCF. In comparison, FMS binds M-CSF with only the D2 and D3 domains. The D1 domains of KIT and FMS are swung in opposite directions: KIT-D1 leans toward the ligand, whereas FMS-D1 points away from the ligand. In addition, the D2 domains, the central domains for ligand binding, are oriented entirely differently in the KIT and FMS complexes. FMS-D2 and KIT-D2 differ by ≈180° vertically, and KIT-D2 is higher than FMS-D2 relative to their ligands (Fig. 2*C*). Consequently, the KIT and FMS D2 domains use entirely different regions of the Ig domain to contact ligand: KIT-D2 contacts SCF with the face of the CFG β-sheet, whereas FMS-D2 contacts M-CSF with the CD and EF loops. To test whether the observed FMS-D2 orientation is indeed important for M-CSF:FMS binding, or just a crystal packing artifact overriding a weak M-CSF:FMS interface, we mutated a FMS residue (Arg-146 → Glu) at the M-CSF:FMS-D2 interface, and measured the binding between M-CSF and the mutant FMS-D1-D5 (supporting information (SI) Fig. S1). The mutation abolished the M-CSF:FMS binding, even when the D4 and D5 domains of FMS are present, proving that the novel FMS D2 orientation is physiologically relevant.

Interestingly, when the D1 and D2 domains of KIT and FMS are taken out of the context of the complexes, they as a whole can be superimposed to each other (Fig. 2*D*). This is consistent with the observation that in both KIT and FMS, D1 and D2 form a rigid, integral region linked by extensive hydrophobic interactions. Hence, the different D1 orientation between KIT and FMS is largely determined by the different ligand-binding orientation of D2 as a result of rotation of the rigid D1-D2 module. Although the D3 domains of KIT and FMS are approximately at the same orientation, KIT-D3 is higher than FMS-D3 relative to their ligands, and is ≈5° more swung-out. Consequently, FMS-D3 is more vertical than KIT-D3 in the complex, which probably makes it easier for the FMS D4 and D5 domains from two receptor chains to form interreceptor contacts.

The different ligand-recognition modes used by KIT and FMS are surprising, especially because of the sequence conservation among class III RTKs (the sequence of KIT is 30% identical to FMS, 25% to PDGFRs, and 20% to FLT3) and their 4-helix-bundle ligands (SCF is 14% identical to M-CSF and 10% to FLT3L). In comparison, the sequence identities between the class I hematopoietic cytokine receptors and between their ligands are often far lower (e.g., 13% identity between IL-2Rβ and gp130, and <5%, or indiscernible, identity between their corresponding ligands IL-2 and IL-6), but their site I recognition, between the cytokine A and C helices and the receptor CRH module, is conserved family-wide.

M-CSF:FMS Interaction. The M-CSF:FMS interface is formed between a flat face on one side of M-CSF, approximately at equal distances from the dimerization interface and from the tail, and the region around the D2-D3 junction on FMS (Fig. 3*A*). The flat face of M-CSF consists of the B and C helices, and the N-terminal segment preceding helix A, whereas the D2 and D3 domains of FMS present inter-β-strand loops for the interface. Because the FMS D2 and D3 domains are oriented relatively straight to, and largely separated from each other, and the linker peptide is located outside the interface, the surfaces contributed by D2 and D3 are discontinuous. The M-CSF:FMS interface therefore can be described as two largely separated sites, site 1, the site between M-CSF and FMS-D2, and site 2, the site between M-CSF and FMS-D3. Overall, ≈1,740 Å^2 of solvent-accessible surface area is buried between each M-CSF and FMS, which can be divided into 900 Å^2 for site 1 and 840 Å^2 for site 2. The interface is mostly hydrophilic, with salt bridges and hydrogen-bonds out-numbering hydrophobic contacts (Table S1). Similar to SCF:KIT binding, charge complementarity appears to have a role in M-CSF:FMS recognition, because the FMS-binding surface on M-CSF is highly acidic, and the M-CSF-binding regions of FMS, overall, are slightly basic (Fig. 3*B*).

The site 1 interface consists of helix B (residue 55–66) and helix C (residues 79–85) of M-CSF, and the CD loop (residues 141–151) and the EF loop (residue 168–173) of FMS-D2 (Fig. 3*C*). It encompasses 3 salt bridges, 4 hydrogen bonds, and a number of van der Waals interactions (Table S1). All 3 salt bridges are of medium range (3.4–3.7 Å), but not close enough to form specific hydrogen bonds. With the long, flexible nature of the sidechains of the charged residues, these medium-range salt bridges alone are unlikely to accurately align M-CSF and FMS-D2 at the interface. In comparison, the hydrogen bonds at

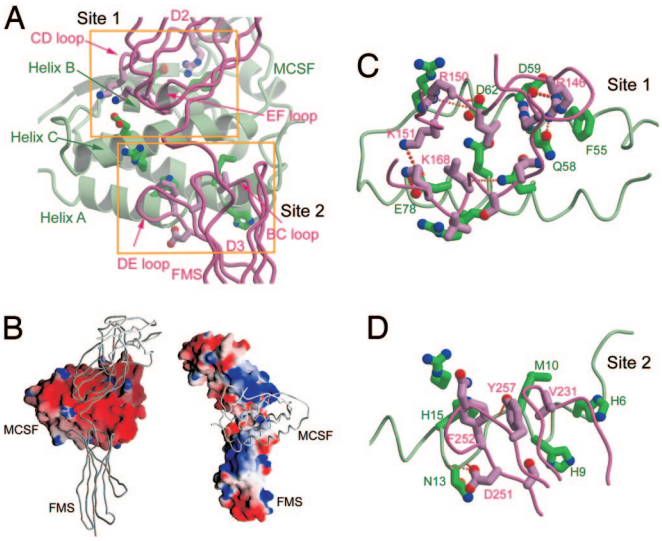

Fig. 3. The interaction between M-CSF and FMS. (*A*) An overview of the M-CSF:FMS interface, with FMS colored in pink and M-CSF in green. (*B*) GRASP surface potential models showing the charge distribution at the interface. (*C*) Close-up view of the site 1 interface between FMS-D2 and the M-CSF B and C helices. (*D*) Close-up view of the site 2 interface between FMS-D3 and the N-terminal segment of M-CSF.

site 1, mostly involving mainchain atoms, are more capable of aligning the two highly hydrophilic surfaces into non-sliding positions. In particular, the sidechains of M-CSF Asp-62 and FMS Arg-150 do not form salt bridges, but instead extend in an anti-parallel fashion to form hydrogen bonds with the mainchain atoms of the other residue. Another notable contact is the interaction between FMS Arg-146 and a patch of 3 residues (Phe-55, Gln-58 and Asp-59) extending from the M-CSF helix B, where the two terminal atoms (Nη1 and Nη2) of FMS Arg-146 form a hydrogen bond with M-CSF Gln-58 and a salt bridge with M-CSF Asp-59 respectively, placing its guanidine group parallel to the aromatic ring of M-CSF Phe-55, thus forming a cation-π interaction (Fig. 3*C* and Fig. S2). This contact has an indispensable role in M-CSF:FMS binding, as shown by the entire loss of binding upon the FMS Arg-146 → Glu mutation (Fig. S1).

The smaller site 2 interface consists of the N-terminal segment of M-CSF (residues 6–15) and the FMS-D3 BC and DE loops (residues 231–232 and 250–257) (Fig. 3*D*). There are 3 hydrogen bonds at this interface, all involving the mainchain of M-CSF (Table S1). The DE loop of FMS-D3 interacts with the near-helix-A part of the M-CSF N-terminal segment, providing terminal sidechain atoms for the 3 hydrogen bonds, and most of the van der Waals interaction between M-CSF and FMS-D3. The BC loop of FMS-D3 only contributes to a small number of van der Waals interactions with the M-CSF N terminus. In particular, the FMS Val-231 and the M-CSF Met-10 form the only interaction between 2 hydrophobic residues at the entire M-CSF:FMS interface.

The composition of the M-CSF:FMS interface is consistent with previous mutagenesis data on M-CSF (24), and is also consistent with the thermodynamic profile of M-CSF:FMS-D1–D3 binding (Fig. 1*B*), which shows a weak affinity contributed by both a small enthalpic decrease and a small entropic increase. Although there is no lack of salt bridges and hydrogen bonds at the interface, the salt bridges are outside the preferred range, and the enthalpy decrease brought by the hydrogen bonds is likely compromised by the burial of two mostly hydrophilic surfaces, which need to break the protein–water hydrogen-bond network existing at the unbound surfaces. The small entropic

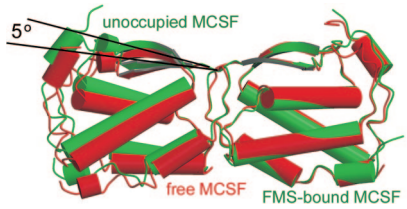

Fig. 4. The M-CSF conformational change upon FMS-D1–D3 binding. Comparison between the free M-CSF dimer (red) and the FMS-D1–D3-bound M-CSF dimer (green) shows that FMS-D1–D3 binding of 1 M-CSF protomer induces a rotational (5°) conformational change of the unoccupied M-CSF protomer.

gain likely results from burying the small number of hydrophobic residues, such as Phe-55; Met-10 of M-CSF; and Leu-170, Leu-149, Val-231, Phe-252 of FMS, albeit most of these residues are not involved in hydrophobic contact.

The M-CSF:FMS interaction is not conserved in the class III RTK family. As mentioned above, the M-CSF:FMS-D2 interaction is entirely different from the SCF:KIT-D2 interaction as a result of FMS-D2 and KIT-D2 using the opposite sides of the Ig domain for binding. Although the D3 domains of KIT and FMS both use the DE loops and the BC loop to contact ligand, there is no similarity in the pattern of hydrogen bonds and van der Waals interaction between these two complexes. Notably, the DE loop of KIT-D3 is 7 aa longer than that of FMS-D3, and KIT-D3 is higher up than FMS-D3 for contacting ligand (Fig. 2*C*), resulting in more intimate interaction between KIT-D3 and SCF than between FMS-D3 and M-CSF.

The M-CSF conformational change upon FMS-D1–D3 binding. The existence of a stable 2:1 M-CSF:FMS-D1–D3 complex suggests that the binding affinity at the second M-CSF:FMS binding site is significantly lower than at the first site, possibly resulting from conformational changes imposed by the binding at the first site. Although the overall structure of the M-CSF dimer bound to FMS is similar to the structure of free M-CSF (18), there is a notable difference in the relative angle between the two M-CSF protomers. Fig. 4 shows that in the FMS-bound M-CSF dimer, the angle between two protomers is increased by ≈5°, which rotates the unbound M-CSF protomer in the complex toward the membrane-distal side. Interestingly, this type of rotation has also been observed for SCF upon KIT binding (23), although its effect has not been further studied. The M-CSF dimer likely also undergoes local conformational changes upon FMS binding. Although the backbone of M-CSF appear rigid, the sidechains of M-CSF at the FMS-binding site may have substantial flexibility, as evidenced by the wide array of sidechain conformational differences between the occupied and the unoccupied M-CSF protomers (Fig. S3). These differences suggest that the M-CSF sidechains, especially at the edge of the FMS-binding site, can be subject to rearrangement upon FMS binding.

The reduced FMS-D1–D3-binding at the second site, if enabled by M-CSF conformational changes, may be a case of negative cooperativity akin to the insulin receptor/insulin binding (26) and the glycoprotein hormone receptor/ligand binding (27). The negative cooperativity in ligand-receptor binding is probably a way of inviting additional factors, such as receptor–receptor interaction and the participation of coreceptors, to the regulation of signal transduction. It should be noted that although the two M-CSF:FMS binding sites may exhibit negative cooperativity, it is undetectable if the receptor–ligand interactions and receptor-receptor interactions are not investigated separately. Most earlier, cell-based studies used entire D1-D5 constructs (28, 29), whose affinities for M-CSF, aided by D4-D5 interactions, are high enough to conceal the difference at the two M-CSF:FMS binding sites.

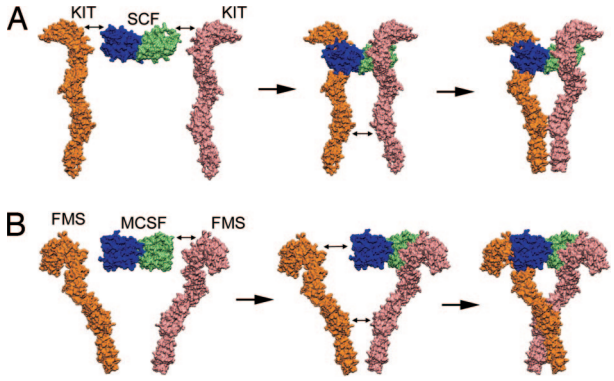

Fig. 5. A model for diverse dimerization and activation mechanisms of the class III RTKs. (*A*) Dimerization and activation are sequential events for KIT. KIT is dimerized directly by the high-affinity binding of SCF at the SCF:KIT interfaces, which in turn enables the membrane-proximal D4 and D5 domains to form secondary contact after a lateral movement. (*B*) Dimerization and activation are concurrent events for FMS. An M-CSF dimer recruits a single FMS in the first step. In the second step, the D4-D5 receptor-receptor interaction and the M-CSF:FMS interaction at the second site enable each other through enthalpic and entropic compensation, allowing the completion of a dimerized and activated complex. The FMS D1-D5 models were created by superimposing KIT D3-D5 (from PDB entry 2E9W) onto FMS D3 and then constructing a chimera of FMS-D1–D3 and the superimposed IT-D4-D5.

Various Assemblies of Class III RTK Signaling Complexes. The biochemical and structural evidence of a partial but stable M-CSF:FMS-D1–D3 complex provides insight into the mechanism of assembly of the cell surface M-CSF:FMS complex (Fig. 5). The first 3 domains, D1, D2, and D3, of FMS appear to contain all of the structural elements necessary for binding M-CSF, and the D4 and D5 domains are unlikely to participate in receptor–ligand contact. The M-CSF dimer is capable of initially binding to the D1-D2-D3 region of one FMS, albeit at low affinity, but is incapable of dimerizing two FMS D1-D2-D3 segments, likely due to the reduced second-site affinity resulting from M-CSF conformational changes. Loading the second FMS awaits the establishment of D4 and D5 receptor–receptor contacts. Because FMS–FMS binding alone is also weak, as evidenced by the absence of oligomerization of soluble FMS-D1-D5 in gel filtration analysis (Fig. 1*A*) and the rapid dimer-monomer transition of endogenous FMS in cultured macrophages (29), the receptor–receptor binding and the M-CSF:FMS binding at the second site most likely happen concurrently and interdependently. Given that binding at the second M-CSF:FMS site may be entropically unfavorable, but that the FMS-D4-D5 brings in large enthalpic changes, a compensation between entropy and enthalpy is likely to happen during the second step of complex formation. In this 2-step assembly mechanism, where a partial complex is formed first and the second copy of receptor is then recruited, dimerization and activation of FMS both happen at the second step (Fig. 5).

Hence, there are profound differences between FMS and KIT, 2 members of the class III RTK family, in their assembly mechanisms. First, as discussed above, the receptor–ligand binding mode is not conserved between KIT and FMS. In particular, the central domain for ligand binding, D2, which among all of the extracellular domains mediates the largest number of specific interactions with ligand, can use entirely difference sides of the domain for binding ligands belonging to the same subgroup of hematopoietic cytokines. The use of entirely different regions on D2 for ligand binding also dictates the differences of D1 in ligand binding. It has been well known that the same group of receptors can use different sites to bind different groups of ligands, e.g., T cell receptor binds MHC and superantigen at different sites, and the same type of ligands can use different sites to bind different groups of receptors, e.g., nerve growth factor binds TrkA and p75 at different sites. However, the utilization of different sites when both the receptors and the ligands belong to the same groups, as shown in SCF:KIT and M-CSF:FMS, is extremely rare. Second, the SCF:KIT and M-CSF:FMS complexes are formed in different mechanistic steps (Fig. 5). The formation of the full SCF:KIT complex also takes two steps, but the first step is the dimerization of two receptors by the dimeric ligand, and the second step, where conformational change allows the formation of D4-D5 receptor-receptor contact, allows the receptor to be activated. The separation of dimerization and activation of KIT is dissimilar to the FMS case where the formation of a partial complex is followed by concurrent dimerization/activation. The inability of M-CSF to dimerize FMS without the aid of FMS D4-D5 is likely due to both the weak nature of the M-CSF:FMS interface and the M-CSF conformational changes. In comparison, SCF binds KIT strongly, and even if the SCF conformational change has a negative influence, the binding at the second site may not be weakened enough to prevent dimerization of KIT, as supported by the existence of 2:2 SCF:KIT-D1–D3 complexes without D4-D5 (22). To compensate for the weak M-CSF:FMS interface and the negative influence of M-CSF conformational changes, FMS D4-D5 probably forms much stronger receptor-receptor interactions than KIT D4-D5 does. Indeed, our calorimetric data indicates that the addition of FMS D4-D5 enhances affinity by 50-fold, and brings a large enthalpic decrease in M-CSF:FMS binding. In comparison, KIT-D1–D3 binds to SCF with precisely the same thermodynamic parameters as does KIT-D1-D5 (30), suggesting the KIT D4-D5 receptor-receptor interaction and the KIT activation are secondary to receptor-ligand binding, and is most likely imposed by the proximity of two receptors.

The structures of the M-CSF:FMS complex, together with the SCF:KIT complex (22, 23), now offer a complex but increasingly clear picture about the formation of class III receptor signaling assemblies. Although all three of the first domains of class III RTKs are needed for ligand binding, D1 may or may not be directly involved in ligand binding, but forms an integral module with D2. D2 has at least two possible orientations for ligand binding. Whether there is additional way of orientating D2 in the complex is unclear, but the likelihood cannot be discounted given that the sequences of FMS and KIT are closer to each other than to the PDGFR-α, PDGFR-β, and FLT3. Whatever the D1 and D2 orientations are in the various complexes, the structures of the signaling complexes are likely to converge at the D3 level. The D4 and D5 domains of various class III RTKs may form interreceptor interactions with surface patches at similar positions, but the configuration and the strength of these interactions may vary considerably. The D4–D5 interactions of one member of this class of receptors is secondary and not required for dimerization, whereas for another member, it is necessary for the formation or stabilization of receptor dimers. It is still unclear whether the D4 and D5 domains of FMS, FLT3, and PDGFRs undergo large-scale lateral conformational changes to bring the C termini of two receptor ectodomains closer, as with KIT (23). However, if such a conformational change exists, it should always contribute to the formation of receptor–receptor interactions.

Finally, The M-CSF:FMS complex represents a simple case in which the ligand alone cannot dimerize receptors and relies on receptor–receptor interactions to complete the signaling assembly. Such a mechanism should be commonplace in biochemistry, especially in cell-surface receptor/ligand interactions. Therefore, the 2-step, sequential-loading, and receptor-aided assembly mechanism, represented by M-CSF:FMS, may be widely applicable to a

variety of cell-surface receptors, especially those with weak ligand–receptor interfaces or those with multiple levels of regulation.

Methods

Construct Design, Expression, and Crystallization. All constructs were cloned into the pAcGP67A baculovirus expression vector, expressed in Hi5 cells, and crystallized as described in *SI Materials and Methods*.

Data Collection and Structure Determination. The crystallographic data were measured and processed, and the structure was determined as described in *SI Materials and Methods*. Crystallographic data statistics are listed in Table S2.

Isothermal Titration Calorimetry. Calorimetric titrations were carried out on a VP-ITC calorimeter (MicroCal, Northhampton, MA) at 30 °C as detailed in *SI Materials and Methods*. The data were processed with MicroCal Origin software, Version 5.0.

ACKNOWLEDGMENTS. X.H. is supported by the National Institutes of Health Grant 1R01GM078055. The Structural Biology Facility is supported by the R.H. Lurie Comprehensive Cancer Center of Northwestern University. Data were measured at the LS-CAT beamline 21-ID-D at the Advanced Photon Source (APS), Argonne, IL. Use of the APS is supported by U.S. Department of Energy Contract W-31-109-Eng-38.

1. Pixley FJ, Stanley ER (2004) CSF-1 regulation of the wandering macrophage: Complexity in action. *Trends Cell Biol* 14:628–638.
2. Donner L, Fedele LA, Garon CF, Anderson SJ, Sherr CJ (1982) McDonough feline sarcoma virus: Characterization of the molecularly cloned provirus and its feline oncogene (v-fms). *J Virol* 41:489–500.
3. Sherr CJ, *et al.* (1985) The c-fms proto-oncogene product is related to the receptor for the mononuclear phagocyte growth factor, CSF-1. *Cell* 41:665–676.
4. Chitu V, Stanley ER (2006) Colony-stimulating factor-1 in immunity and inflammation. *Curr Opin Immunol* 18:39–48.
5. Teitelbaum SL, Ross FP (2003) Genetic regulation of osteoclast development and function. *Nat Rev Genet* 4:638–649.
6. Dai XM, *et al.* (2002) Targeted disruption of the mouse colony-stimulating factor 1 receptor gene results in osteopetrosis, mononuclear phagocyte deficiency, increased primitive progenitor cell frequencies, and reproductive defects. *Blood* 99:111–120.
7. Shimano H, *et al.* (1990) Human monocyte colony-stimulating factor enhances the clearance of lipoproteins containing apolipoprotein B-100 via both low density lipoprotein receptor-dependent and -independent pathways in rabbits. *J Biol Chem* 265:12869–12875.
8. Danks L, Sabokbar A, Gundle R, Athanasou NA (2002) Synovial macrophage-osteoclast differentiation in inflammatory arthritis. *Ann Rheum Dis* 61:916–921.
9. Rosenfeld ME, *et al.* (1992) Macrophage colony-stimulating factor mRNA and protein in atherosclerotic lesions of rabbits and humans. *Am J Pathol* 140:291–300.
10. Levine JA, Jensen MD, Eberhardt NL, O'Brien T (1998) Adipocyte macrophage colony-stimulating factor is a mediator of adipose tissue growth. *J Clin Invest* 101:1557–1564.
11. Aharinejad S, *et al.* (2004) Colony-stimulating factor-1 blockade by antisense oligonucleotides and small interfering RNAs suppresses growth of human mammary tumor xenografts in mice. *Cancer Res* 64:5378–5384.
12. Lin EY, Nguyen AV, Russell RG, Pollard JW (2001) Colony-stimulating factor 1 promotes progression of mammary tumors to malignancy. *J Exp Med* 193:727–740.
13. Wyckoff J, *et al.* (2004) A paracrine loop between tumor cells and macrophages is required for tumor cell migration in mammary tumors. *Cancer Res* 64:7022–7029.
14. Rettenmier CW, Roussel MF (1988) Differential processing of colony-stimulating factor 1 precursors encoded by two human cDNAs. *Mol Cell Biol* 8:5026–5034.
15. Price LK, Choi HU, Rosenberg L, Stanley ER (1992) The predominant form of secreted colony stimulating factor-1 is a proteoglycan. *J Biol Chem* 267:2190–2199.
16. Bazan JF (1993) Emerging families of cytokines and receptors. *Curr Biol* 3:603–606.
17. Jiang X, *et al.* (2000) Structure of the active core of human stem cell factor and analysis of binding to its receptor kit. *EMBO J* 19:3192–3203.
18. Pandit J, *et al.* (1992) Three-dimensional structure of dimeric human recombinant macrophage colony-stimulating factor. *Science* 258:1358–1362.
19. Savvides SN, Boone T, Andrew Karplus P (2000) Flt3 ligand structure and unexpected commonalities of helical bundles and cystine knots. *Nat Struct Biol* 7:486–491.
20. Zhang Z, Zhang R, Joachimiak A, Schlessinger J, Kong XP (2000) Crystal structure of human stem cell factor: Implication for stem cell factor receptor dimerization and activation. *Proc Natl Acad Sci USA* 97:7732–7737.
21. Schlessinger J (2000) Cell signaling by receptor tyrosine kinases. *Cell* 103:211–225.
22. Liu H, Chen X, Focia PJ, He X (2007) Structural basis for stem cell factor-KIT signaling and activation of class III receptor tyrosine kinases. *EMBO J* 26:891–901.
23. Yuzawa S, *et al.* (2007) Structural basis for activation of the receptor tyrosine kinase KIT by stem cell factor. *Cell* 130:323–334.
24. Koths K Structure-function studies on human macrophage colony-stimulating factor (M-CSF). *Mol Reprod Dev* 46:31–37, 1997; discussion 37–38.
25. Wang ZE, Myles GM, Brandt CS, Lioubin MN, Rohrschneider L (1993) Identification of the ligand-binding regions in the macrophage colony-stimulating factor receptor extracellular domain. *Mol Cell Biol* 13:5348–5359.
26. DeMeyts P, Bainco AR, Roth J (1976) Site-site interactions among insulin receptors. Characterization of the negative cooperativity. *J Biol Chem* 251:1877–1888.
27. Urizar E, *et al.* (2005) Glycoprotein hormone receptors: Link between receptor homodimerization and negative cooperativity. *EMBO J* 24:1954–1964.
28. Carlberg K, Rohrschneider L (1994) The effect of activating mutations on dimerization, tyrosine phosphorylation and internalization of the macrophage colony stimulating factor receptor. *Mol Biol Cell* 5:81–95.
29. Li W, Stanley ER (1991) Role of dimerization and modification of the CSF-1 receptor in its activation and internalization during the CSF-1 response. *EMBO J* 10:277–288.
30. Lemmon MA, Pinchasi D, Zhou M, Lax I, Schlessinger J (1997) Kit receptor dimerization is driven by bivalent binding of stem cell factor. *J Biol Chem* 272:6311–6317.